# Controlled Supramolecular Assembly of Micelle-Like Gold Nanoparticles in PS-*b*-P2VP Diblock Copolymers via Hydrogen Bonding

Se Gyu Jang,[†] Edward J. Kramer,[*,†,‡,§] and Craig J. Hawker[*,†,§,||]

[†]Materials Research Laboratory, [‡]Department of Chemical Engineering, [§]Department of Materials, and [||]Department of Chemistry and Biochemistry, University of California, Santa Barbara, California, 93106, United States

S *Supporting Information*

ABSTRACT: We report a facile strategy to synthesize amphiphilic gold (Au) nanoparticles functionalized with a multilayer, micelle-like structure consisting of a Au core, an inner hydroxylated polyisoprene (PIOH) layer, and an outer polystyrene shell (PS). Careful control of enthalpic interactions via a systematic variation of structural parameters, such as number of hydroxyl groups per ligand (N_{OH}) and styrene repeating units (N_{PS}) as well as areal chain density of ligands on the Au-core surface (Σ), enables precise control of the spatial distribution of these nanoparticles. This control was demonstrated in a lamellae-forming poly(styrene-*b*-2-vinylpyridine) (PS-*b*-P2VP) diblock copolymer matrix, where the favorable hydrogen-bonding interaction between hydroxyl groups in the PIOH inner shell and P2VP chains in the PS-*b*-P2VP diblock copolymer matrix, driving the nanoparticles to be segregated in P2VP domains, could be counter balanced by the enthalpic penalty of mixing of the PS outer brush with the P2VP domains. By varying N_{OH}, N_{PS}, and Σ, the nanoparticles could be positioned in the PS or P2VP domains or at the PS/P2VP interface. In addition, the effect of additives interfering with the hydrogen-bond formation between hydroxyl groups on Au nanoparticles and P2VP chains in a diblock copolymer matrix was investigated, and an interesting pea-pod-like segregation of Au nanoparticles in PS domains was observed.
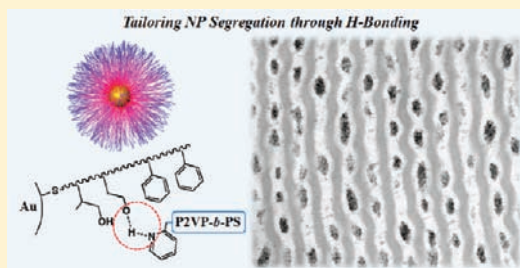
INTRODUCTION

Ligand molecules tethered on the surface of inorganic nanoparticles play an important role in the synthesis and application of nanoparticles due to their dramatic influence over surface properties.[1,2] Tailoring of nanoparticle surfaces with ligands is therefore a key factor for stabilizing nanoparticles in various solvents as well as for controlling hierarchical assembly of nanoparticles to give functional materials. The incorporation of inorganic nanoparticles into block copolymer matrices to give self-assembled, microphase-separated periodic structures has been intensively studied to create novel functional hybrid materials, such as high-performance catalysts, photonic crystals, chemical sensors, and electronic devices.[3–7] Precise control of nanoparticle segregation in A-*b*-B block copolymers has been achieved by synthesizing nanoparticles with various ligands, including short aliphatic molecules, A or B homopolymers, mixed A and B homopolymers, and A-*r*-B random copolymers leading to localization of the nanoparticles into either A or B domains or at the A/B interface.[8–18] These approaches are based on minimizing the enthalpic interaction of mixing of nanoparticles into block copolymer matrices by tailoring the nanoparticle surface with components similar to the respective block copolymer domains. Recently, Kim et al. demonstrated that the segregation of nanoparticles can also be precisely controlled by an attractive secondary interaction between nanoparticle cores

and the block copolymer matrix.[15–17,19] For example, the physical adsorption of poly(2-vinylpyridine) (P2VP) chains on the surface of the gold core (Au), allowed by the low areal chain density (Σ) of PS ligands, has been successfully employed to segregate nanoparticles at the interface of poly(styrene-*b*-2-vinylpyridine) (PS-*b*-P2VP) diblock copolymers.

In examining other attractive, nonbonded interactions, our attention was drawn to hydrogen bonding.[20,21] Due to its specific, directional, and reversible characteristics, hydrogen bonding has been widely used for supramolecular self-assembly of polymers and inorganic molecules.[7,22] Although the typical single hydrogen-bond strength (5–30 kJ/mol) is much less than covalent bonds (250–800 kJ/mol), significant favorable interactions can be obtained through the formation of multiple hydrogen bonds. This enables self-healing polymeric materials, which is an emerging goal in materials science.[23,24] In addition, blending of block copolymers with homopolymers having multiple complementary hydrogen bonds has been used to induce interesting order—order morphology transitions without macrophase separation of homopolymers from block copolymer domains.[25–31] Hydrogen bonding also has been used for the selective segregation of nanoparticles in block copolymer domains. Yeh et al.

Scheme 1. Synthesis of Au Nanoparticles[a]
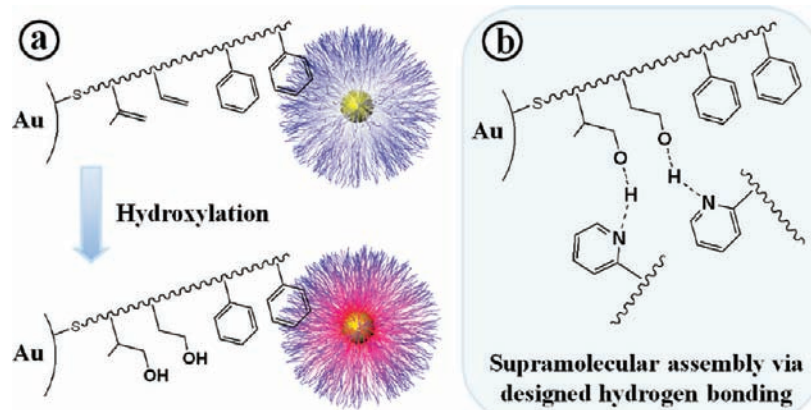
[a] (a) Schematic illustration of creation of micelle-like gold (Au) nanoparticles consisting of hydrophilic inner shell with hydroxyl groups (PIOH) and hydrophobic polystyrene (PS) outer brush. Double bonds on thiol-terminated PS-*b*-PI-SH tethered on gold nanoparticle surface were converted to hydroxyl groups via hydroboration reaction. (b) Schematic illustration of designed hydrogen-bonding formation between hydroxyl group on the nanoparticle ligand and pyridine group on P2VP block in PS-*b*-P2VP block copolymer.

controlled the localization of CdS nanoparticles into poly-(ethylene oxide) (PEO) domains in poly(styrene-*b*-ethylene oxide) (PS-*b*-PEO) through favorable hydrogen-bonding interactions between hydroxyl groups on CdS nanoparticles and PEO blocks.[32] Similarly, Lin et al. employed a hydrogen-bonding strategy to incorporate Au (or silicon) nanoparticles, at very high volume fractions ($\sim$ 36 vol%), into PS-*b*-PEO or poly(ethylene oxide-*b*-propylene oxide-*b*-ethylene oxide) (PEO-*b*-PPO-*b*-PEO) block copolymers.[33] Although the use of hydrogen bonding to control nanoparticle segregation has been demonstrated, its effectiveness for the coassembly of nanoparticles in block copolymer matrices is limited by the inherent solubility of nanoparticles covered with hydroxyl groups (hydrogen-bonding donor) in only polar solvents, such as water or dimethylformamide (DMF). In turn this leads to difficulties in processing of the nanoparticle/block copolymer mixture. To increase the solubility and processability of nanoparticles in nonpolar solvents, Li et al. synthesized Au nanoparticles with mixed dodecane-thiol and 11-mercapto-1-undecanol ligands.[34] The nanoparticles showed good solubility in toluene and segregated in poly(4-vinylpyridine) (P4VP) domains and at the PS/P4VP interfaces of poly(styrene-*b*-4-vinylpyridine) (PS-*b*-P4VP) diblock copolymer, respectively, due to hydrogen-bonding interactions between pyridine and hydroxyl groups. However, systematic investigations of the segregation behavior of nanoparticles relating to the areal chain density of ligands on nanoparticle surfaces and the length of ligands, known to be the most important factors in nanoparticle segregation in block copolymer matrices,[15−17] have not been undertaken in hydrogen-bonding induced nanoparticle segregation.

Here, we introduce a facile strategy for the preparation of Au nanoparticles, where the number and the location of hydrogen-bonding donors are controlled and allow for high levels of incorporation while retaining solubility in nonpolar solvents. Mimicking micelle structure, Au nanoparticles were initially functionalized with thiol-terminated poly(styrene-*b*-1,2-/3,4-isoprene) (PS-*b*-PI) diblock copolymer ligands. The double bonds of the 1,2-/3,4-isoprene block were then hydroxylated by a hydroboration reaction[35,36] to give multilayer core−shell nanoparticles with a Au core, an inner shell with hydroxyl groups (PIOH), and an outer

**Table 1. Characterization of Thiol-Terminated Poly(styrene-*b*-1,2-/3,4-isoprene)**

	PS (GPC)		PS-*b*-PI-SH (GPC)		PI (NMR)[a]	
	M_n (kg/mol)	PDI	M_n (kg/mol)	PDI	M_n (kg/mol)	N_v[b]
PS$_{43}$-*b*-I$_7$-SH	4.5	1.25	6.5	1.15	0.5	7
PS$_{34}$-*b*-I$_{10}$-SH	3.5	1.15	4.3	1.14	0.7	9
PS$_{26}$-*b*-I$_{12}$-SH	2.7	1.33	3.8	1.15	0.8	11
PS$_{29}$-*b*-I$_{21}$-SH	3.0	1.13	4.6	1.08	1.4	20
PS$_{30}$-*b*-I$_{26}$-SH	3.1	1.29	5.2	1.21	1.8	25

[a] Obtained from end-group analysis by ^{1}H NMR. [b] Average number of pendant double bonds per chain obtained from the number of 1,2- and 3,4-isoprene units calculated from the ^{1}H NMR.

shell of PS chains. Owing to the PS shell, the nanoparticles were highly soluble over a range of molecular weights of ligands in non-polar organic solvents, such as dichloromethane (DCM) and chloroform, which are also good and nonselective solvents for the PS-*b*-P2VP block copolymer. As a result, sample preparation by drop-casting or solvent annealing of composites could be accomplished without any concerns of nanoparticle aggregation during processing. A library of nanoparticles with various structural parameters, such as length of PS, number of hydroxyl groups per ligand, and areal chain density of ligands, was synthesized, and the effects of each parameter on the segregation of nanoparticles in PS-*b*-P2VP were systematically studied. The high degree of structural control in this system also allowed the influence of small molecule, hydrogen-bonding additives to be studied in detail.

■ RESULTS AND DISCUSSION

Scheme 1 illustrates the strategy developed for the synthesis of Au nanoparticles with a controlled, multilayer structure. Thiol-terminated poly(styrene-*b*-1,2-/3,4-isoprene) (PS-*b*-PI-SH) was prepared by sequential anionic polymerization of styrene and isoprene monomers with the polymerization of isoprene performed in THF to produce primarily 1,2 and 3,4 additions of isoprene monomers (>95%) rather than 1,4 addition (<5%).[37]
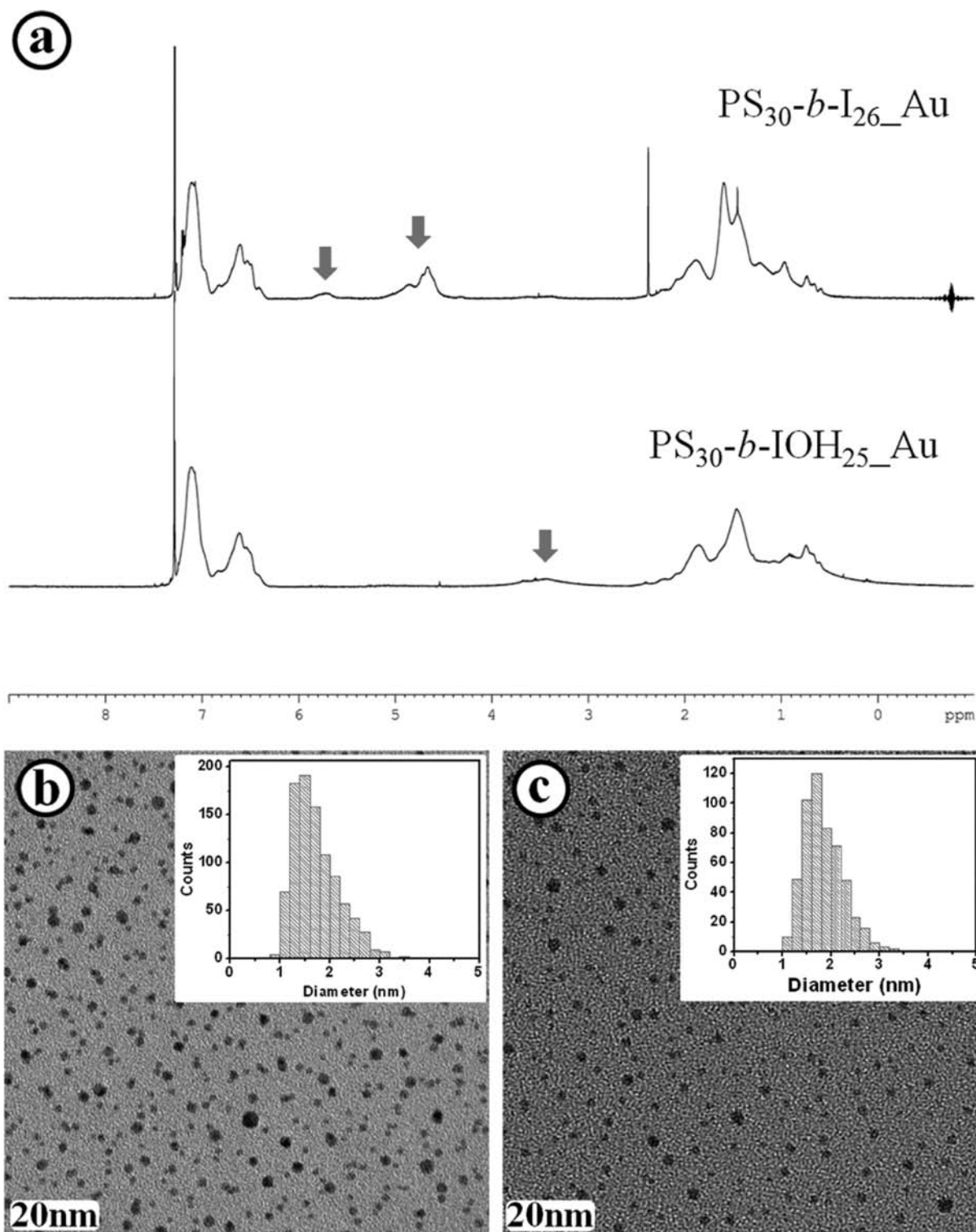
Figure 1. (a) ^{1}H NMR spectra of Au nanoparticles covered with PS$_{30}$-b-I$_{26}$-SH (PS$_{30}$-b-I$_{26}$-Au) (top) and PS$_{30}$-b-IOH$_{25}$-Au_1 nanoparticles after hydroxylation (bottom) in CDCl$_3$. Disappearance of broad peaks centered at 4.7 and 5.7 ppm from double bonds in 1,2-/3,4-isoprene and a new peak centered at 3.4 ppm after hydroxylation reveals that the hydroboration reaction was high yielding. (b and c) TEM micrographs and corresponding size distributions before hydroxylation (b, PS$_{30}$-b-I$_{26}$-Au, D_{core} = 1.7 ± 0.4 nm) and after hydroxylation (c, PS$_{30}$-b-IOH$_{25}$-Au_1, D_{core} = 1.7 ± 0.5 nm).

See Table 1 for results. Using the thiol-terminated diblock copolymer ligands, Au nanoparticles with a double-bond-rich inner polyisoprene (PI) shell and a polystyrene (PS) outer layer were synthesized by a modified Brust method,[38,39] followed by hydroxylation of the double bonds in the PI inner block by a hydroboration reaction (Scheme 1).[36] Owing to the hydrophobic PS outer layer, the Au nanoparticles could be dispersed in organic solvents, such as DCM and chloroform, which are good

Table 2. Characterization of Hydroxylated Au Nanoparticles

|	ligand	D_{core} (nm)[a]	Σ (chains/nm^2)[b]	Σ_{eff} (chains/nm^2)[c]	N_{PS}/N_{OH}[d]
PS_{43}-b-IOH_7-Au_1	PS_{43}-b-I_7-SH	2.4 ± 0.5	1.9	0.6	6.1
PS_{34}-b-IOH_9-Au_1	PS_{34}-b-I_{10}-SH	2.3 ± 0.6	1.2	0.4	3.8
PS_{34}-b-IOH_9-Au_2	PS_{34}-b-I_{10}-SH	2.1 ± 0.8	1.3	0.4	3.8
PS_{26}-b-IOH_{11}-Au_1	PS_{26}-b-I_{12}-SH	2.5 ± 0.4	1.2	0.4	2.4
PS_{29}-b-IOH_{20}-Au_1	PS_{29}-b-I_{21}-SH	3.1 ± 1.0	0.7	0.2	1.5
PS_{29}-b-IOH_{20}-Au_2	PS_{29}-b-I_{21}-SH	2.8 ± 0.7	1.1	0.3	1.5
PS_{29}-b-IOH_{20}-Au_3	PS_{29}-b-I_{21}-SH	2.4 ± 0.5	2.2	0.6	1.5
PS_{30}-b-IOH_{25}-Au_1	PS_{30}-b-I_{26}-SH	1.7 ± 0.4	1.8	0.3	1.2

[a] Mean diameter obtained from image analysis based on TEM images for at least 300 Au nanoparticles. [b] Calculated from TGA analysis and D_{core}. [c] Estimated from the root-mean-square end-to-end distance of the collapsed polyvinylalcohol in poor solvent. [d] Calculated from number of styrene repeating units (N_{PS}) and hydroxyl groups (N_{OH}) per ligand.

solvents for PS-b-P2VP diblock copolymer, even though the inner PIOH block with a large number of hydrogen-bond donating hydroxyl groups is hydrophilic. This allows a mixture of Au nanoparticles and PS-b-P2VP diblock copolymers to be dissolved in chloroform, drop-cast, and annealed with saturated DCM vapor. Scheme 1b illustrates the hydrogen-bond-mediated supramolecular assembly between hydroxyl groups on the PIOH inner shell (hydrogen-bonding donor) and pyridine groups (hydrogen-bonding acceptor) on the P2VP block of PS-b-P2VP diblock copolymer. A key to the design of these nanoparticles is the ability to control the structural features of these materials, which allows the favorable hydrogen-bonding interactions that attract the nanoparticles to the P2VP phase of microphase-separated PS-b-P2VP diblock copolymer domains to offset the enthalpic penalty due to mixing of Au nanoparticles covered with PS outer brushes into the P2VP phase, an enthalpic penalty that favors nanoparticle placement in the PS domains. Therefore, the segregation and location of the nanoparticles in the PS-b-P2VP diblock copolymer can be controlled by adjusting these enthalphic interactions and corresponding structural features.

The hydroxylation of pendent double bonds in the PIOH inner shell of nanoparticles via hydroboration could be monitored by ^{1}H NMR (Figure 1a). The peaks centered at 4.7 and 5.7 ppm due to the double bonds of the PS_{30}-b-I_{26}-Au nanoparticles were completely absent after hydroboration, as shown in the bottom spectrum (PS_{30}-b-IOH_{25}-Au_1). In addition, a new broad peak centered at 3.4 ppm, corresponding to the protons adjacent to hydroxyl groups, indicates that the hydroxylation of double bonds via hydroboration was high yielding. The broadening of the peaks, especially in the case of protons near the hydroxyl groups, is due to increased spin—spin relaxation (T_2) as a result of the restricted motion of the protons closely packed on the surface of a Au nanoparticle.[40,41] To demonstrate that hydroboration did not result in loss of polymer ligands or aggregation of the Au cores, transmission electron microscopy (TEM) images and histograms showing the size distributions of Au nanoparticles taken before (PS_{30}-b-I_{26}-Au) and after hydroxylation (PS_{30}-b-IOH_{25}-Au_1) are provided in Figure 1b and c. PS_{30}-b-IOH_{25}-Au_1 nanoparticles demonstrate little, if any, change in nanoparticle size or physical properties. In this example, the mean core diameter of the hydroxylated nanoparticle PS_{30}-b-IOH_{25}-Au_1 ($D_{core} = 1.7 \pm 0.5$ nm) was essentially the same as the starting PS_{30}-b-I_{26}-Au ($D_{core} = 1.7 \pm 0.4$ nm) nanoparticles. In addition, Au nanoparticles with various other diblock copolymer ligands, as listed in Table 2, also showed no changes after hydroxylation and retained good solubility in chloroform and DCM.

To investigate the effect of hydrogen-bond formation on the lateral distribution of nanoparticles in a lamellae-forming PS-b-P2VP block copolymer matrix (199 kg/mol), composite samples with Au nanoparticles before (PS_{26}-b-I_{12}-Au) and after hydroxylation (PS_{26}-b-IOH_{11}-Au_1) were characterized by cross-sectional TEM micrographs and related histograms (Figure 2) with the white stripes being PS domains and the black (or gray) stripes corresponding to iodine-stained P2VP domains. Due to the PS outer layer and hydrophobic double-bond-rich PI inner shell, PS_{26}-b-I_{12}-Au nanoparticles (appearing as black dots) were segregated into the PS domains, as shown in Figure 2a (histogram in Figure 2c). In addition, a significant number of PS_{26}-b-I_{12}-Au nanoparticles were macrophase separated from the diblock copolymer domains (Figure 2a inset). In contrast, the location of the Au nanoparticles after hydroxylation (PS_{26}-b-IOH_{11}-Au_1 was dramatically different, with the nanoparticles segregating to the PS/P2VP interface, as shown in Figure 2b (histogram in Figure 2d). No macrophase separation of the nanoparticles from the diblock copolymer domains was observed, even at a slightly higher nanoparticle volume fraction ($\phi_p \sim 12.5\%$) when compared to the composite sample with the nonhydroxylated PS_{26}-b-I_{12}-Au ($\phi_p \sim 11\%$). Furthermore, the normalized lamellar domain thickness $h(\phi_p)/h_0$, which is the ratio of lamellar domain thickness (half the lamellar period) $h(\phi_p)$ at a volume fraction ϕ_p to the lamellar domain thickness h_0 for $\phi_p = 0$, was reduced to 0.76 due to the surfactant action of the hydroxylated Au nanoparticles adsorbed at the interface of the diblock copolymer domains.[15,19] The adsorption of PS_{26}-b-IOH_{11}-Au_1 nanoparticles to the PS/P2VP interface indicates that the hydrogen bonding between the hydroxyl groups in the PIOH shell and the pyridyl units of the P2VP pulls the nanoparticles from the PS domains and stabilizes them at the PS/P2VP interface.

The segregation behavior of Au nanoparticles with PS ligands is highly dependent on the areal chain density (Σ) of ligands.[15,16,19] For example, the interfacial adsorption of Au nanoparticles with a low areal chain density ($<\Sigma_c$, the critical areal chain density) of nanoparticle ligands caused by the favorable interaction between P2VP and the Au surface has been reported by Kim et al. To examine the effect of Σ on the segregation behavior of these multilayer nanoparticles, Au nanoparticles with the same PS_{29}-b-IOH_{20}-SH ligand but with various values of Σ were synthesized and blended with PS-b-P2VP diblock copolymer. From cross-sectional TEM micrographs, as shown in Figure 3a (PS_{29}-b-IOH_{20}-Au_1, 0.7 chains/nm^2), 3b (PS_{29}-b-IOH_{20}-Au_2, 1.1 chains/nm^2), and 3c (PS_{29}-b-IOH_{20}-Au_3, 2.2 chains/nm^2), for
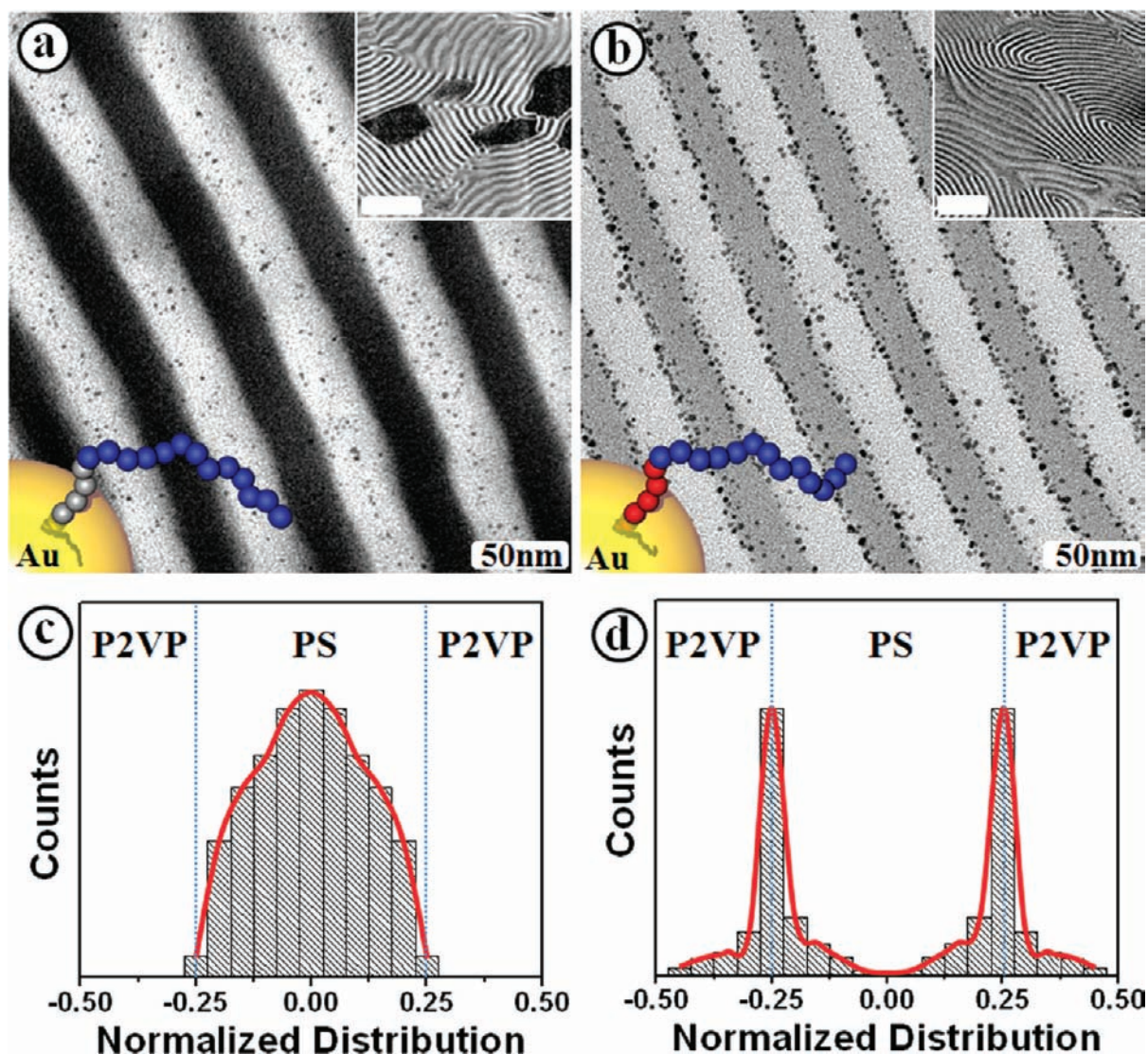
Figure 2. Cross-sectional TEM micrographs of lamellae-forming PS-*b*-P2VP block copolymer (199 kg/mol) containing Au nanoparticles whose ligands are: (a) nonhydroxylated (PS$_{26}$-*b*-I$_{12}$-Au) and (b) hydroxylated (PS$_{26}$-*b*-IOH$_{11}$-Au_1). The areal chain density Σ of PS$_{26}$-*b*-I$_{12}$-Au is 1.2 chains/nm^2. Gray, blue, and red spheres on the nanoparticles in the illustration at the bottom left of TEM images represent double-bond-rich PI, PS, and hydroxylated PIOH, respectively. The composite samples were annealed with DCM vapor for 2 days. Volume fractions of nanoparticles (ϕ_p) in PS-*b*-P2VP are: (a) 11% and (b) 12.5%. Scale bars in the insets are 500 nm. (e and f) Histograms showing nanoparticle distributions in PS-*b*-P2VP microdomains obtained from the TEM micrographs in (a) and (b), respectively. The normalized domain size refers to the distance of the nanoparticle from the center of the PS domain divided by the size of a single period of the structure formed by PS-*b*-P2VP, and blue dotted lines located at +0.25 and −0.25 represent the interfaces between PS and P2VP. For accurate measurements, the samples were tilted to align the direction of the lamellar planes and electron beam of the microscope to reduce the broadening of interfaces caused by misalignment of the electron beam.

the lowest Σ (PS$_{29}$-*b*-IOH$_{20}$-Au_1), the segregation of PS$_{29}$-*b*-IOH$_{20}$-Au_1 nanoparticles into P2VP domains might be expected as a result of favorable interactions between P2VP chains and Au surfaces as well as hydroxyl groups of ligands. In contrast, segregation of PS$_{29}$-*b*-IOH$_{20}$-Au_3 nanoparticles with the highest Σ might be segregated into the PS domain of the diblock copolymer as a result of efficient shielding of hydrogen bonding by densely packed PS brushes.[42] However, in all three examples, the nanoparticles were segregated at the PS/P2VP interfaces regardless of Σ. The entropic stretching penalty of block copolymer chains due to the nanoparticle incorporation into block copolymer domains, which is more significant in the case of larger nanoparticles in size, is known to be an important factor affecting segregation behavior of nanoparticles.[43,44] However, the multilayer

Au nanoparticles in Figure 3a have a broad range of core diameters but yet were segregated at the interface regardless of their core diameter. This result indicates that an entropic stretching penalty is not the major factor in determining the segregation location of the multilayer Au nanoparticles as long as the particles are 5 nm or less in core-diameter. In addition to the entropic stretching penalty of block copolymer chains caused by nanoparticle incorporation, there are at least four more main enthalpic interactions determining the segregation location of nanoparticles in PS-*b*-P2VP diblock copolymers: the enthalpic penalties of mixing by PS brushes into P2VP domains ($\Delta H_{\text{mix,PS-P2VP}}$) and PIOH inner shells into PS domains ($\Delta H_{\text{mix,PIOH-PS}}$) as well as enthalpic gains caused by hydrogen bonding (ΔH_{HB}) and P2VP adsorption on Au surfaces (ΔH_{ad}). When Σ is low enough, the penetration of P2VP chains
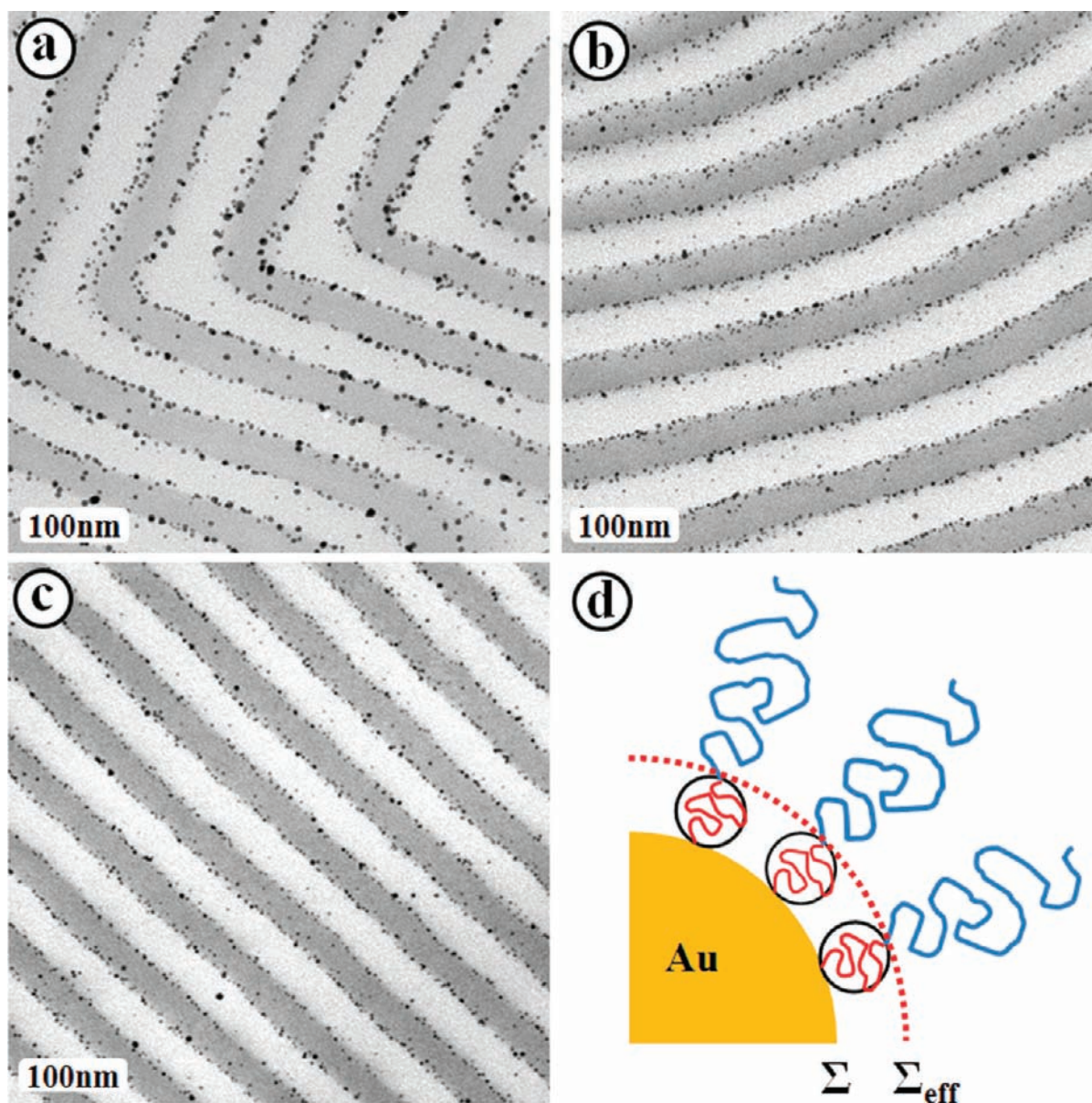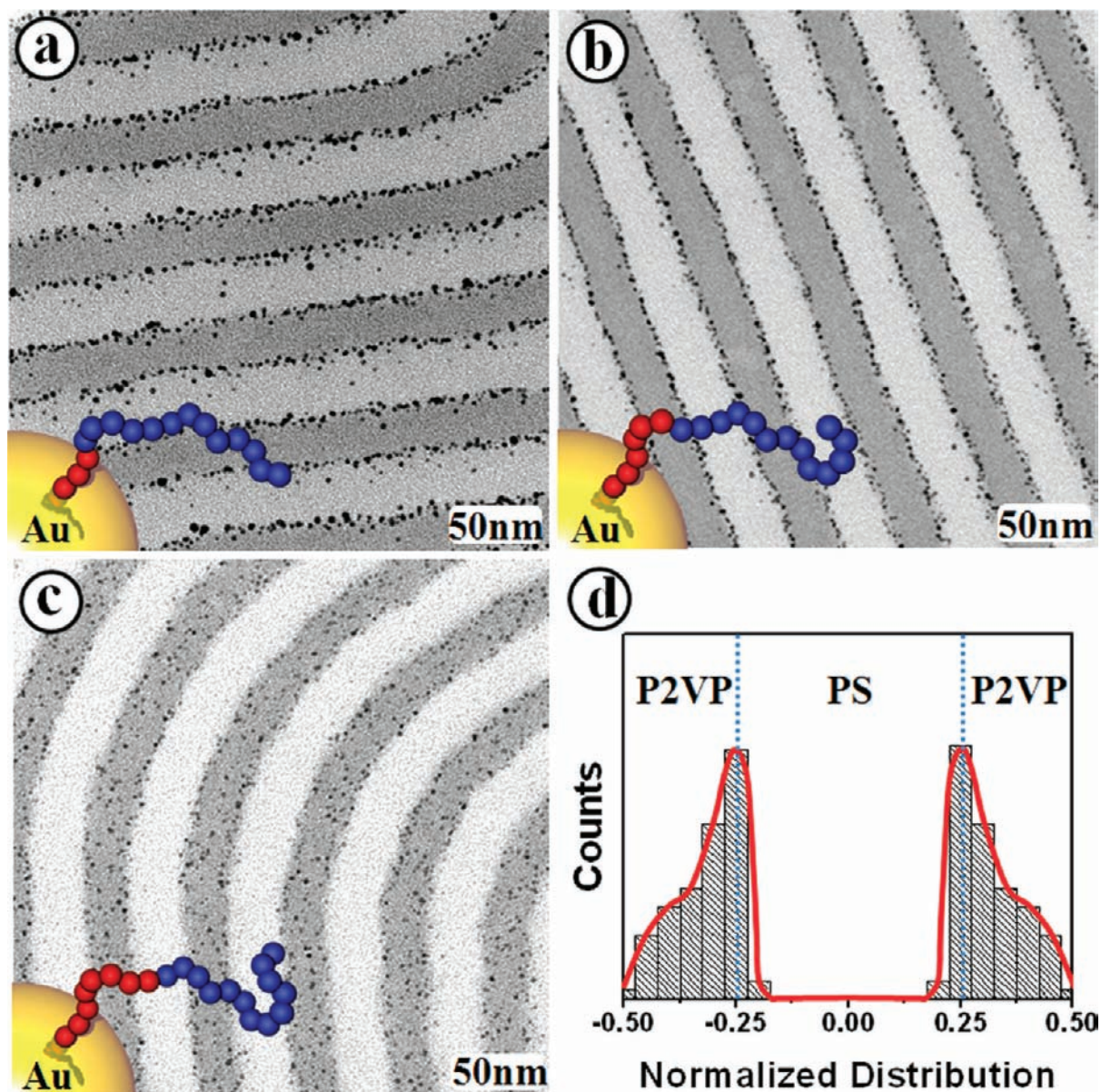
Figure 3. Cross-sectional TEM micrographs of lamellae-forming PS-*b*-P2VP block copolymer (199 kg/mol) containing Au nanoparticles covered with the same ligand (PS$_{29}$-*b*-IOH$_{20}$-SH) but various areal chain densities: (a) 0.7 chains/nm^2 (PS$_{29}$-*b*-IOH$_{20}$-Au_1, $\phi_p \sim$ 5%), (b) 1.1 chains/nm^2 (PS$_{29}$-*b*-IOH$_{20}$-Au_2, $\phi_p \sim$ 7%), and (c) 2.2 chains/nm^2 (PS$_{29}$-*b*-IOH$_{20}$-Au_3, $\phi_p \sim$ 19%). (d) Illustration of the effective areal chain density at the interface between inner hydroxylated PIOH block and outer brush (Σ_{eff}). PIOH inner blocks containing hydroxyl groups are collapsed as globules due to the unfavorable interaction with DCM used for solvent annealing of composites.

through the PS outer brush is significant. Therefore, $|\Delta H_{HB}|$ and $|\Delta H_{mix,PS-P2VP}|$ are dependent on the thickness of the PIOH and PS layers, respectively, rather than the number of ligands on the Au surface related to Σ. Although there might be a considerable interaction between P2VP chains and both the Au surface (ΔH_{ad}) and PIOH (ΔH_{HB}), due to the low Σ of PS$_{29}$-*b*-IOH$_{20}$-Au_1 (Figure 3a, $\Sigma \sim$ 0.7 chains/nm^2) nanoparticles, the segregation of PS$_{29}$-*b*-IOH$_{20}$-Au_1 nanoparticles at the interface reflects that the sum of enthalpic gain, due to the formation of hydrogen bonding and P2VP adsorption on the Au surface ($|\Delta H_{HB} + \Delta H_{ad}|$), is comparable to $|\Delta H_{mix,PS-P2VP}|$. Considering the high density of ligands on the Au surface, the adsorption of PS$_{29}$-*b*-IOH$_{20}$-Au_3 nanoparticles at the interface (Figure 3c) indicates that there still exists hydrogen bonding between P2VP and hydroxyl groups in the

inner shell even in the case of nanoparticles with the highest Σ. The easy access of P2VP chains to the hydroxyl groups through the densely packed PS brush even at high Σ can be explained by considering the effective areal chain density (Σ_{eff}) of ligands on the surface of the PIOH shell (Figure 3d). The Σ_{eff} values of each nanoparticle, estimated from the root-mean-square end-to-end distance of the collapsed polyvinylalcohols with similar molecular structures to PIOH in poor solvent are listed in Table 2.[45] The Σ_{eff} of PS$_{29}$-*b*-IOH$_{20}$-Au_2 and PS$_{29}$-*b*-IOH$_{20}$-Au_3 are much lower than Σ on the surface of the Au-core. Lower Σ_{eff} results in better contact of P2VP to hydroxyl groups and more hydrogen-bond formation driving the nanoparticles to PS/P2VP interface.

The segregation location of these novel, multilayer Au nanoparticles is highly correlated with the enthalpic energy balances,
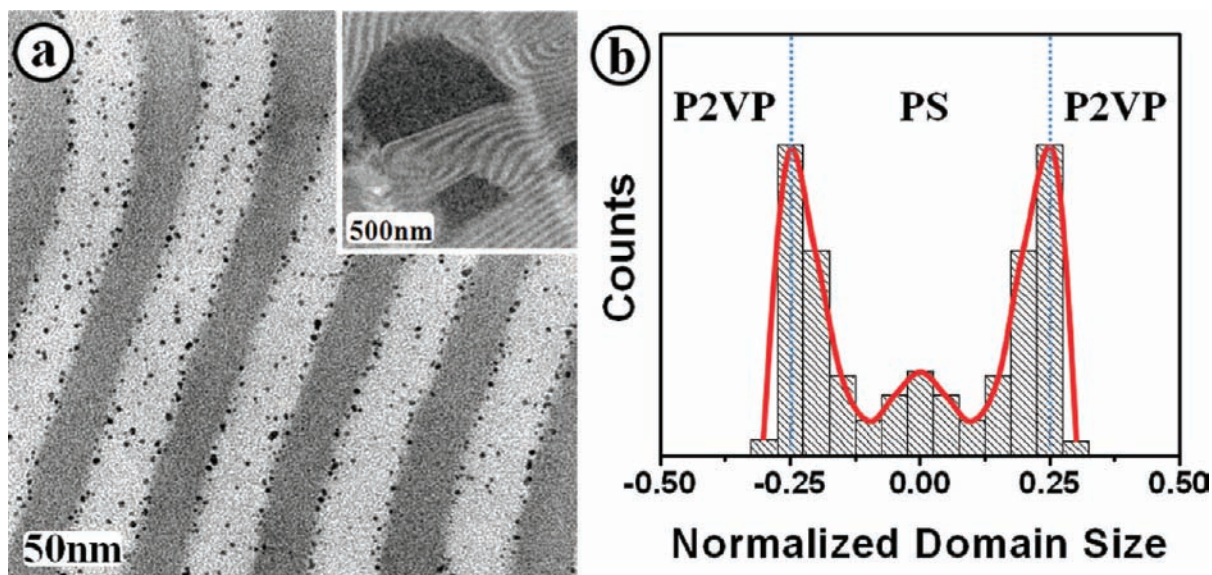
Figure 4. Cross-sectional TEM micrographs of lamellae-forming PS-*b*-P2VP block copolymer (199 kg/mol) containing Au nanoparticles with fixed length of PS (~ 3 kg/mol) but various numbers of hydroxyl groups on the PIOH inner block: (a) 9 (PS_{34}-*b*-IOH_9-Au_1, $\phi_p \sim 11\%$, $\Sigma \sim 1.2$ chains/nm^2), (b) 20 (PS_{29}-*b*-IOH_{20}-Au_2, $\phi_p \sim 7\%$, $\Sigma \sim 1.1$ chains/nm^2), and (c) 25 (PS_{30}-*b*-IOH_{25}-Au_1, $\phi_p \sim 19\%$, $\Sigma \sim 1.8$ chains/nm^2). Blue and red spheres on the nanoparticles in the illustration at the bottom left of the TEM images represent PS and hydroxylated PIOH, respectively. (d) Histogram showing nanoparticle distribution in PS-*b*-P2VP microdomains obtained from the TEM micrographs in (c).

especially between $|\Delta H_{HB}|$ and $|\Delta H_{mix,PS\text{-}P2VP}|$. To investigate the effect of PIOH chain length related to $|\Delta H_{HB}|$ on the segregation location of nanoparticles, three different nanoparticles with fixed PS brush length (fixed $|\Delta H_{mix,PS\text{-}P2VP}|$, $M_n \sim 3$ kg/mol) but with various numbers of hydroxyl groups (N_{OH}, various $|\Delta H_{HB}|$) ranging from 9 to 25 per ligand were synthesized and mixed with the PS-*b*-P2VP diblock copolymer matrix. PS_{34}-*b*-IOH_9-Au_1 ($N_{OH} \sim 9$) and PS_{29}-*b*-IOH_{20}-Au_2 ($N_{OH} \sim 20$) nanoparticles in Figure 4a and b, respectively, were localized at the PS/P2VP interface. However, PS_{30}-*b*-IOH_{25}-Au_1 ($N_{OH} \sim 25$) nanoparticles were segregated in both P2VP domains and interfaces as shown in the cross-sectional TEM micrograph in Figure 4c (histogram in Figure 4d), suggesting that $|\Delta H_{HB} + \Delta H_{ad}|$ is similar to or greater than $|\Delta H_{mix,PS\text{-}P2VP}|$.

The coexistence of nanoparticles at the interface and in the P2VP phase is due to the distribution of core size, Σ, and length of PS and PIOH blocks on nanoparticles as reported previously.[17] Considering the fact that the Σ of PS_{30}-*b*-IOH_{25}-Au_1 ($\Sigma \sim 1.8$ chains/nm^2) is higher than those of PS_{34}-*b*-IOH_9-Au_1 ($\Sigma \sim 1.2$ chains/nm^2) and PS_{29}-*b*-IOH_{20}-Au_2 ($\Sigma \sim 1.1$ chains/nm^2), the segregation of PS_{30}-*b*-IOH_{25}-Au_1 nanoparticles in the P2VP phase may be due to the increase in $|\Delta H_{HB}|$ rather than the increase in $|\Delta H_{ad}|$. These observations demonstrate that the segregation and the location of hydroxylated nanoparticles in a PS-*b*-P2VP diblock copolymer matrix are highly dependent on the number of hydroxyl groups, N_{OH}.

To further demonstrate the tunability of these multilayer Au nanoparticles in controlling nanoparticle segregation in block

Figure 5. (a) Cross-sectional TEM micrograph and (b) a histogram showing distribution of PS_{43}-b-IOH_7-Au_1 nanoparticles ($\Sigma \sim 1.9$ chains/nm^2) in lamellae-forming PS-b-P2VP block copolymer (199 kg/mol). Au nanoparticles are covered with ligands consisting of 4.5 kg/mol PS and 0.5 kg/mol ($\sim$7 hydroxyl groups) PIOH blocks. The nanoparticles are mainly segregated to the PS/P2VP interface as shown in the histogram in (b). However, a significant amount of nanoparticles is segregated into the PS domain or macrophase separated as shown in the inset in (a).

copolymer domains, nanoparticles were specifically designed to be localized in PS domains. The initial strategy examined was to increase the $|\Delta H_{mix,PS-P2VP}|$ and reduce the $|\Delta H_{HB}|$ by the synthesis of Au nanoparticles (PS_{43}-b-IOH_7-Au_1, $\Sigma \sim 1.9$ chains/nm^2) with diblock copolymer ligands of longer PS ($N_{PS} \sim 43$) and shorter PIOH ($N_{OH} \sim 7$) blocks. The resulting PS_{43}-b-IOH_7-Au_1 nanoparticles were observed to be localized in PS domains as well as at PS/P2VP interfaces as shown in the cross-sectional TEM micrographs in Figure 5a and the histogram in Figure 5b, with macrophase separation also being present (Figure 5a inset image). This observation reflects the significant decrease in contribution from hydrogen bonding which is effectively shielded by the long and dense PS brushes as well as the decrease in overall number of hydroxyl groups. From this experimental result, we find an interesting feature of the multi-layer Au nanoparticles when compared to Au nanoparticles with only PS homopolymer ligands. Based on Kim's experimental results, the critical areal chain density of Au nanoparticles ($\Sigma_c \sim M_n^{-0.6\pm0.1}$) with a 4.5 kg/mol PS ligand can be estimated as $\sim$1.3 chains/nm^2, which means that the Au nanoparticles with Σ lower than 1.3 chains/nm^2 are segregated at the PS/P2VP interfaces.[17] Considering that the hydrogen bonding and the adsorption of P2VP chains on Au-core surfaces are energetically favorable and induce the segregation of nanoparticles to the interface, it is reasonable that the PS_{43}-b-IOH_7-Au_1 nanoparticles with $\Sigma_{eff} \sim 0.6$ chains/nm^2, which is much lower than Σ_c, might be segregated to the interface rather than within PS domains. The segregation of PS_{43}-b-IOH_7-Au_1 nanoparticles in PS domains, even in the case where Σ_{eff} is lower than Σ_c, may be due to difficulty in "Janus" formation of densely packed diblock copolymer ligands on the PS_{43}-b-IOH_7-Au_1 nanoparticle-core surface ($\Sigma \sim 1.9$ chains/nm^2). The driving force to form "Janus" structures of PS homopolymer ligands tethered on Au-core surfaces is the energy gain from the rearrangement of PS ligands to avoid unfavorable interactions between PS brushes and P2VP chains in diblock copolymer chains and to increase favorable
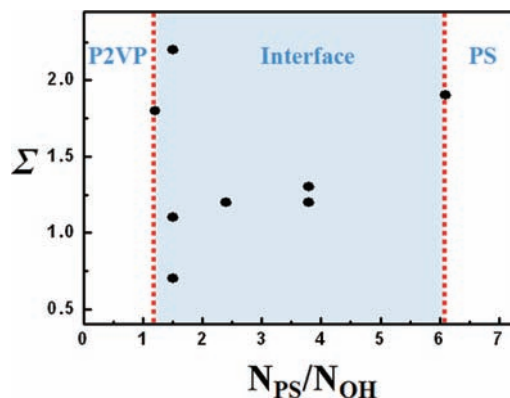

Figure 6. Summary of nanoparticle segregation locations plotted by areal chain density of ligands (Σ) vs N_{PS}/N_{OH}, where N_{PS} is number of styrene repeating units on PS brush, and N_{OH} is number of hydroxyl groups on the PIOH inner block. Nanoparticles are primarily segregated to the PS/P2VP interface when $1.2 < N_{PS}/N_{OH} < 6.1$. However, segregation of nanoparticles into P2VP and PS domains was observed when $N_{PS}/N_{OH} \sim 1.2$ and 6.1, respectively.

interactions between bare gold surfaces and P2VP chains. Therefore, the segregation of PS_{43}-b-IOH_7-Au_1 nanoparticles in the PS domains is primarily due to effective shielding of the P2VP chains from interacting with the hydroxyl groups near the Au surface by the PS brush.

The segregation behaviors were explored by varying Σ, the number of repeating units of PS (N_{PS}) and PIOH (N_{OH}) blocks of ligands. Figure 6 summarizes the location of various nanoparticles plotted by Σ and N_{PS}/N_{OH}. The majority of multilayer Au nanoparticles examined was found to be segregated at the PS/P2VP interface due to strong hydrogen-bond formation when $1.2 < N_{PS}/N_{OH} < 6.1$. Decreasing N_{PS}/N_{OH} ($\sim$1.2) resulted in segregation of nanoparticles to the P2VP domains through a reduction in Σ_{eff} and a corresponding increase in $|\Delta H_{HB} + \Delta H_{ad}|$
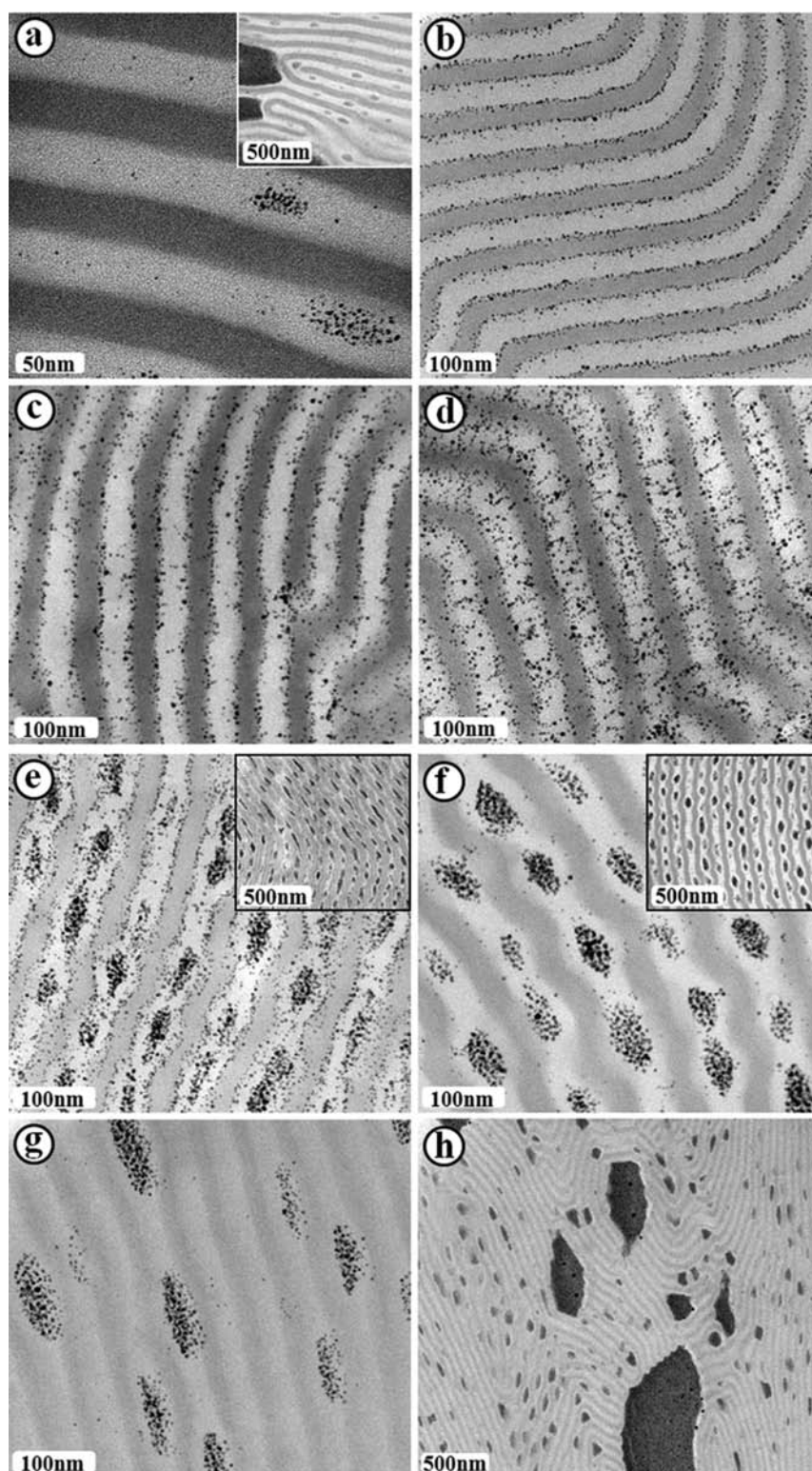
Figure 7. Cross-sectional TEM micrographs of PS-*b*-P2VP block copolymer (199 kg/mol) and hydroxylated Au nanoparticles showing the effect of a 4PPy additive which forms competing hydrogen bonds with hydroxyl groups on nanoparticle ligands. (a) Au nanoparticles with PS_{34}-*b*-I_{10}-SH ligands before hydroxylation of PI block. (b−h) PS_{34}-*b*-IOH_9-Au_1 nanoparticles mixed with various amounts of 4PPy relative to total number of hydroxyl groups on the nanoparticles: (b) 0 molar equiv, (c) 2 molar equiv, (d) 3 molar equiv, (e) 4 molar equiv, (f) 5 molar equiv, and (g and h) 10 molar equiv 4PPy. The initial segregation of Au nanoparticles to the interface (b) was gradually shifted to the PS domain (c and d) and subsequently to the formation of small nanoparticle aggregates which assemble into novel "pea-pod" morphologies. At high loading of 4PPy (g and h), significant nanoparticle aggregation is observed.

over $|\Delta H_{mix,PS-P2VP}|$. The segregation of nanoparticles to the PS domains was observed when N_{PS}/N_{OH} is ca. 6.1 and demonstrates

that shielding of the hydroxyl groups and a subsequent reduction in hydrogen-bonding interactions is possible with a dense PS

16994

dx.doi.org/10.1021/ja206615c |*J. Am. Chem. Soc.* 2011, 133, 16986–16996

outer layer. The trivial effect of Σ on the nanoparticle segregations is mainly due to the significantly low Σ_{eff} values as a result of the increase in N_{OH}. The effect of Σ will be more pronounced when the N_{OH} value goes to zero, as for the Au nanoparticles with only PS ligands demonstrated by Kim et al.[17]

In addition to modulating the effect of hydrogen bonding by varying N_{PS} and N_{OH}, the use of a small molecule which interferes with hydrogen bonding between the PIOH and P2VP chains may be another variable that can be used to control nanoparticle segregation. In addition, the enhanced mobility of small molecule additives may provide opportunities for interesting morphologies of multilayer Au nanoparticles in PS-b-P2VP diblock copolymer matrices to be obtained.[28] For this purpose, 4-phenylpyridine (4PPy) was added to the block copolymer/nanoparticle composites (see Supporting Information Figure S1 for the cross-sectional TEM micrographs of PS-b-P2VP diblock copolymer mixed with various amounts of 4ppy in the absence of Au nanoparticles). It is envisaged that the pyridine group of the small molecule additive would hydrogen bond with the hydroxyl groups within the PIOH shell of the nanoparticle and compete with the P2VP chains, not only screening the hydrogen bonding between the P2VP and the nanoparticle ligands but also modifying the polarity of the PIOH inner shell. As control experiments, Figure 7a shows the segregated Au nanoparticles with PS$_{34}$-b-I$_{10}$-SH ligands before hydroxylation with weak aggregation in PS domains of the diblock copolymer and macrophase separation being observed. In contrast, PS$_{34}$-b-IOH$_9$-Au_1 nanoparticles were segregated to the PS/P2VP interfaces after hydroxylation (Figure 7b). Significantly, nanoparticle segregation could be accurately tuned by varying the amount of 4PPy added to composites, relative to the total number of hydroxyl groups on the nanoparticles mixed with PS-b-P2VP: (c) 2 molar equiv, (d) 3 molar equiv, (e) 4 molar equiv, (f) 5 molar equiv, and (g and h) 10 molar equiv 4ppy (Figure 7c—h). PS$_{34}$-b-IOH$_9$-Au_1 nanoparticles were primarily segregated to the interface when 2 molar equiv of additive was used (Figure 7c). When 3 molar equiv of 4ppy was added (Figure 7d), the population of nanoparticles in PS domains was increased dramatically and hierarchical pea-pod-like segregation of PS$_{34}$-b-IOH$_9$-Au_1 nanoparticles in PS domains (ovulated cylinder morphology parallel to the lamellar domains in 3-D), due to the weak aggregation of nanoparticles into the center of PS domains, was observed in Figure 7e. Further increasing the concentration of 4ppy (5 molar equiv) resulted in no nanoparticles at the interface with the majority of nanoparticles being present in pea-pod-like nanoaggregates within the PS domains. The local swelling of PS domains near the aggregated nanoparticles resulted in the undulation of lamellar domains, and the aggregated nanoparticles formed hexagonal arrangements (Figure 7f). Finally, the same segregation morphology of nanoparticles with Figure 7a was observed in Figure 7g—h when an excess (10 molar equiv) of 4ppy was used, reflecting that hydrogen bonding between PIOH chains in nanoparticle ligands and P2VP chains was completely screened by the additives.

CONCLUSION

Novel core—shell nanoparticles with a Au core and controlled number of hydroxyl groups in the inner shell and PS outer layer, were synthesized via hydroxylation of the pendant double bonds of thiol-terminated poly(styrene-b-1,2-/3,4-isoprene) ligands tethered on Au-core surfaces. By controlling the structure of the block copolymer ligand, the PS outer layer allows the nanoparticles

to be dispersed in nonpolar organic solvents, which is important for blending of the nanoparticles with diblock copolymers as well as for processing. The presence of hydroxyl groups provides an efficient handle to control the segregation behaviors of nanoparticles in a PS-b-P2VP diblock copolymer matrix via hydrogen bonding. Interestingly, the majority of nanoparticle structures examined were strongly adsorbed to the PS/P2VP interfaces as a result of the enthalpic energy balance between the sum of energy gain by hydrogen-bonding formation ($|\Delta H_{HB}|$) as well as adsorption of P2VP chains on Au-core surfaces ($|\Delta H_{ad}|$) and the energy penalty of mixing PS brushes into P2VP domains ($|\Delta H_{mix,PS-P2VP}|$). Increasing N_{OH} resulted in the increase of $|\Delta H_{HB}|$ and the reduction of effective areal chain density of PS brushes at the outer surface of the PIOH inner shell (Σ_{eff}), allowing P2VP chains better access to the hydroxyl groups in the inner shell. As a result, segregation of nanoparticles to the P2VP domains was observed when $N_{OH}/N_{PS} \sim 1.2$. Conversely, segregation of nanoparticles to the PS domains was observed for structures with increased N_{PS}, causing an increase in $|\Delta H_{mix,PS-P2VP}|$ and more efficient shielding of hydroxyl groups by PS brushes ($N_{OH}/N_{PS} \sim 6.1$). Furthermore, the hierarchical pea-pod-like segregation of nanoparticles in PS domains, that has not been obtained by conventional coassembly of nanoparticles and block copolymers, was observed by introducing 4-phenylpyridine as an inhibitor to hydrogen-bond formation between hydroxyl groups on nanoparticles and P2VP chains in PS-b-P2VP diblock copolymers.

■ ASSOCIATED CONTENT

ⓢ Supporting Information. Detailed experimental procedures; cross-sectional TEM micrographs of lamellae-forming PS-b-P2VP block copolymer (199 kg/mol) mixed with various amounts of 4PPy only. This material is available free of charge via the Internet at http://pubs.acs.org.

■ AUTHOR INFORMATION

Corresponding Author
edkramer@mrl.ucsb.edu; hawker@mrl.ucsb.edu

■ ACKNOWLEDGMENT

■ REFERENCES

(1) Daniel, M. C.; Astruc, D. *Chem. Rev.* **2004**, *104*, 293–346.

(2) Shan, J.; Tenhu, H. *Chem. Commun.* **2007**, *44*, 4580–4598.

(3) Bockstaller, M. R.; Thomas, E. L. *J. Phys. Chem. B* **2003**, *107*, 10017–10024.

(4) Cheng, J. Y.; Ross, C. A.; Chan, V. Z. H.; Thomas, E. L.; Lammertink, R. G. H.; Vancso, G. J. *Adv. Mater.* **2001**, *13*, 1174–1178.

(5) Jaramillo, T. F.; Baeck, S. H.; Cuenya, B. R.; McFarland, E. W. *J. Am. Chem. Soc.* **2003**, *125*, 7148–7149.

(6) Mui, S. C.; Trapa, P. E.; Huang, B.; Soo, P. P.; Lozow, M. I.; Wang, T. C.; Cohen, R. E.; Mansour, A. N.; Mukerjee, S.; Mayes, A. M.; Sadoway, D. R. *J. Electrochem. Soc.* **2002**, *149*, A1610–A1615.

(7) Warren, S. C.; Messina, L. C.; Slaughter, L. S.; Kamperman, M.; Zhou, Q.; Gruner, S. M.; DiSalvo, F. J.; Wiesner, U. *Science* **2008**, *320*, 1748–1752.

(8) (a) Bockstaller, M. R.; Thomas, E. L. *Phys. Rev. Lett.* **2004**, *93*, 166106. (b) Yu, H.; Luo, Z. *J. Polym. Sci., Part A: Polym. Chem.* **2010**, *48*, 5570–5580.

(9) (a) Chiu, J. J.; Kim, B. J.; Yi, G. R.; Bang, J.; Kramer, E. J.; Pine, D. J. *Macromolecules* **2007**, *40*, 3361–3365. (b) Wang, W.; Cao, H.; Zhu, G.; Wang, P. *J. Polym. Sci., Part A: Polym. Chem.* **2010**, *48*, 1782–1790. (c) van Berkel, K. Y.; Hawker, C. J. *J. Polym. Sci., Part A: Polym. Chem.* **2010**, *48*, 1594–1606. (d) Oh, H.; Green, P. F. *Nat. Mater.* **2009**, *8*, 139–143.

(10) Chiu, J. J.; Kim, B. J.; Kramer, E. J.; Pine, D. J. *J. Am. Chem. Soc.* **2005**, *127*, 5036–5037.

(11) (a) Chung, H.; Ohno, K.; Fukuda, T.; Composto, R. J. *Nano Lett.* **2005**, *5*, 1878–1882. (b) Hickey, R. J.; Sanchez-Gyatan, B. L.; Cui, W. H.; Composto, R. J.; Fryd, M.; Wayland, B. B.; Park, S. J. *Small* **2010**, *6*, 48–51.

(12) (a) Kang, H.; Detcheverry, F. A.; Mangham, A. N.; Stoykovich, M. P.; Daoulas, K. C.; Hamers, R. J.; Muller, M.; de Pablo, J. J.; Nealey, P. F. *Phys. Rev. Lett.* **2008**, *100*, 148303. (b) Constanzo, P. J.; Beyer, F. L. *Macromolecules* **2007**, *40*, 3996–4001.

(13) Kim, B. J.; Bang, J.; Hawker, C. J.; Chiu, J. J.; Pine, D. J.; Jang, S. G.; Yang, S. M.; Kramer, E. J. *Langmuir* **2007**, *23*, 12693–12703.

(14) Kim, B. J.; Chiu, J. J.; Yi, G. R.; Pine, D. J.; Kramer, E. J. *Adv. Mater.* **2005**, *17*, 2618–2622.

(15) Kim, B. J.; Fredrickson, G. H.; Hawker, C. J.; Kramer, E. J. *Langmuir* **2007**, *23*, 7804–7809.

(16) Kim, B. J.; Bang, J.; Hawker, C. J.; Kramer, E. J. *Macromolecules* **2006**, *39*, 4108–4114.

(17) Kim, B. J.; Fredrickson, G. H.; Kramer, E. J. *Macromolecules* **2008**, *41*, 436–447.

(18) (a) Park, S. C.; Kim, B. J.; Hawker, C. J.; Kramer, E. J.; Bang, J.; Ha, J. S. *Macromolecules* **2007**, *40*, 8119–8124. (b) Böker, A.; Lin, Y.; Chiapperini, K.; Horowitz, R.; Thompson, M.; Carreon, V.; Xu, T.; Abetz, C.; Skaff, H.; Dinsmore, A. D.; Emrick, T.; Russell, T. P. *Nat. Mater.* **2004**, *3*, 302–306. (c) Hu, Y.; Chen, D.; Park, S.; Emrick, T.; Russell, T. P. *Adv. Mater.* **2010**, *22*, 2583–2587.

(19) Kim, B. J.; Fredrickson, G. H.; Bang, J.; Hawker, C. J.; Kramer, E. J. *Macromolecules* **2009**, *42*, 6193–6201.

(20) Zimmerman, S. C.; Corbin, F. S. *Mol. Self-Assembly* **2000**, *96*, 63–94.

(21) Binder, W. H.; Zirbs, R. *Adv. Polym. Sci.* **2007**, *207*, 1–78.

(22) Zhao, Y.; Thorkelsson, K.; Mastroianni, A. J.; Schilling, T.; Luther, J. M.; Rancatore, B. J.; Matsunaga, K.; Jinnai, H.; Wu, Y.; Poulsen, D.; Frechet, J. M. J.; Alivisatos, A. P.; Xu, T. *Nat. Mater.* **2009**, *8*, 979–985.

(23) Blaiszik, B. J.; Kramer, S. L. B.; Olugebefola, S. C.; Moore, J. S.; Sottos, N. R.; White, S. R. *Ann. Rev. Mater. Res.* **2010**, *40*, 179–211.

(24) Cordier, P.; Tournilhac, F.; Soulie-Ziakovic, C.; Leibler, L. *Nature* **2008**, *451*, 977–980.

(25) Noro, A.; Matsushita, Y.; Lodge, T. P. *Macromolecules* **2008**, *41*, 5839–5844.

(26) (a) Tang, C. B.; Sivanandan, K.; Stahl, B. C.; Fredrickson, G. H.; Kramer, E. J.; Hawker, C. J. *ACS Nano* **2010**, *4*, 285–291. (b) Tang, C.; Lennon, E. M.; Fredrickson, G. H.; Kramer, E. J.; Hawker, C. J. *Science* **2008**, *322*, 429–432.

(27) Dobrosielska, K.; Wakao, S.; Takano, A.; Matsushita, Y. *Macromolecules* **2008**, *41*, 7695–7698.

(28) (a) Bousquet, A.; Ibarboure, E.; Papon, E.; Labrugère, C.; Rodríguez-Hernández, J. *J. Polym. Sci., Part A: Polym. Chem.* **2010**, *48*, 1952–1961. (b) Yang, P.; Wang, L.; Tang, C.; Lin, C. *J. Polym. Sci., Part A: Polym. Chem.* **2010**, *48*, 764–774.

(29) Coleman, M. M.; Painter, P. C. *Prog. Polym. Sci.* **1995**, *20*, 1–59.

(30) Feldman, K. E.; Kade, M. J.; de Greef, T. F. A.; Meijer, E. W.; Kramer, E. J.; Hawker, C. J. *Macromolecules* **2008**, *41*, 4694–4700.

(31) Feldman, K. E.; Kade, M. J.; Meijer, E. W.; Hawker, C. J.; Kramer, E. J. *Macromolecules* **2010**, *43*, 5121–5127.

(32) Yeh, S. W.; Chang, Y. T.; Chou, C. H.; Wei, K. H. *Macromol. Rapid Commun.* **2004**, *25*, 1680–1686.

(33) Lin, Y.; Daga, V. K.; Anderson, E. R.; Gido, S. P.; Watkins, J. J. *J. Am. Chem. Soc.* **2011**, *133*, 6513–6516.

(34) Li, Q. F.; He, J. B.; Glogowski, E.; Li, X. F.; Wang, J.; Emrick, T.; Russell, T. P. *Adv. Mater.* **2008**, *20*, 1462–1466.

(35) Andruzzi, L.; Chiellini, E.; Galli, G.; Li, X. F.; Kang, S. H.; Ober, C. K. *J. Mater. Chem.* **2002**, *12*, 1684–1692.

(36) Wang, J. G.; Mao, G. P.; Ober, C. K.; Kramer, E. J. *Macromolecules* **1997**, *30*, 1906–1914.

(37) Worsfold, D. J.; Bywater, S. *Can. J. Chem.-Rev. Can. Chim.* **1964**, *42*, 2884–2892.

(38) Brust, M.; Walker, M.; Bethell, D.; Schiffrin, D. J.; Whyman, R. *J. Chem. Soc.-Chem. Comm.* **1994**, 801–802.

(39) Jang, S. G.; Khan, A.; Dimitriou, M. D.; Kim, B. J.; Lynd, N. A.; Kramer, E. J.; Hawker, C. J. *Soft Matter* **2011**, *7*, 6255–6263.

(40) Hongyu, Z.; Fenfang, D.; Xi, L.; Bin, Z.; Wei, L.; Bing, Y. *J. Phys. Chem. C* **2008**, *112*, 19360–19366.

(41) Hostetler, M. J.; Wingate, J. E.; Zhong, C. J.; Harris, J. E.; Vachet, R. W.; Clark, M. R.; Londono, J. D.; Green, S. J.; Stokes, J. J.; Wignall, G. D.; Glish, G. L.; Porter, M. D.; Evans, N. D.; Murray, R. W. *Langmuir* **1998**, *14*, 17–30.

(42) Pruthtikul, R.; Coleman, M. M.; Painter, A. C.; Tan, N. B. *Macromolecules* **2001**, *34*, 4145–4150.

(43) Bockstaller, M. R.; Lapetnikov, Y.; Margel, S.; Thomas, E. L. *J. Am. Chem. Soc.* **2003**, *125*, 5276–5277.

(44) Blockstaller, M. R.; Mickiewicz, R. A.; Thomas, E. L. *Adv. Mater.* **2005**, *17*, 1331–1349.

(45) Thormann, E.; Evans, D. R.; Craig, V. S. J. *Macromolecules* **2006**, *39*, 6180–6185.

16996

dx.doi.org/10.1021/ja206615c |*J. Am. Chem. Soc.* 2011, 133, 16986–16996